Further Test of the Tube Dilation Process in Star-Branched *cis*-Polyisoprene: Role of Branching-Point Fluctuation

Yumi Matsumiya and Hiroshi Watanabe*

Institute for Chemical Research, Kyoto University, Uji, Kyoto 611-0011 Japan

Received January 24, 2001; Revised Manuscript Received May 4, 2001

ABSTRACT: In current tube models for entangled polymer chains, the tube representing the topological constraint is considered to move with time. This tube motion results in constraint release (CR) as well as dynamic tube dilation (DTD), the latter occurring as a result of CR-equilibration of the chain. For the DTD process of type-A star chains, a particular relationship between the normalized dielectric and viscoelastic relaxation functions, $\Phi(t)$ and $\mu(t)$, can be derived under an assumption that a fluctuation amplitude of the star-branching point (BP) is smaller than the diameter of the dilated tube. This DTD relationship, $\mu(t) \cong [\Phi(t)]^2$, does not hold for the terminal relaxation of the stars (Watanabe et al. *J. Polym. Sci. B Polym. Phys.* **2000**, *38*, 1024). This result, suggesting failure of the DTD molecular picture, might have been also attributed to breakdown of the assumption utilized in the above derivation. Under this background, this study examined dielectric and viscoelastic properties for a series of type-A *cis*-polyisoprene (PI) star chains having the same arm molecular weights ($M_a \cong 7M_e$) but different arm numbers q (= 4−15). The BP fluctuation should be suppressed, and thus, the DTD relationship should become valid with increasing q *if* the breakdown of the above assumption was the main reason for the observed failure of the DTD relationship. Nevertheless, for the series of star PI, this relationship was found to fail to nearly the same extent irrespective of the q value. This result indicated that the assumption of short-ranged BP fluctuation was not responsible for the observed failure of the DTD molecular picture. Thus, this failure was attributed to incomplete CR-equilibration for the portion of the star arms near BP. Analyses of the $\Phi(t)$ data suggested that this incompleteness was intrinsically related to the broad motional modes of the star arm.

1. Introduction

Entanglement of flexible polymer chains results from topological constraint of the chains. Description of the entanglement effects on the chain dynamics has been an important subject of polymer physics. Early versions of the tube model, the Doi−Edwards model[1−3] for linear chains and the Doi−Kuzuu[4] and Pearson−Helfand[5] models for star-branched chains, represented this constraint as a spatially fixed tube. These models remarkably reproduced qualitative features of those chains. However, quantitative differences remained between the model predictions and experiments.[6−8] Thus, the tube model has been refined/generalized by combining the reptation and/or arm retraction mode (considered in the early models) with the other dynamic modes such as contour length fluctuation (CLF),[6,9,10] constraint release (CR),[6,11] and dynamic tube dilation (DTD).[12−18] The DTD process results from mutual equilibration of neighboring entanglement segments due to their CR motion and leads to a decrease of the number of independently stress-sustaining units (enlarged segments) with increasing time t.[8,12,13] This DTD mechanism is incorporated in recent models[12−18] as an important stress relaxation mechanism. These models describe the viscoelastic behavior of entangled linear/star chains with considerable accuracy, although nonnegligible differences between the model predictions and experiments still remain. Detailed features of those models (including their limitations) are summarized in a recent review.[8]

Despite this theoretical importance of DTD in viscoelastic relaxation, the chain motion during the DTD process itself was not tested experimentally. For this problem, we recently focused on dielectric and viscoelastic relaxation functions $\Phi(t)$ and $\mu(t)$ of monodisperse linear and star chains having so-called type-A dipoles[19] parallel along the chain backbone. These functions differently average the same motion of the chain.[8,20,21] Taking advantage of this difference, we derived an experimentally testable relationship, $\mu(t) \cong [\Phi(t)]^2$ that should hold whenever the tube dilates in the time scale of the chain relaxation.[20,21] For the linear chains, this DTD relationship was derived from general molecular expressions of $\mu(t)$ and $\Phi(t)$ without specific assumptions for the chain motion.[20] On the other hand, for the star chains, the same relationship was obtained under an assumption that the star-branching point fluctuates with an amplitude smaller than the dilated tube diameter $a'(t)$.[21]

We also tested the above DTD relationship for type-A *cis*-polyisoprene (PI) chains. For well-entangled monodisperse linear PI, this relationship was valid for the dielectric and viscoelastic data in the terminal relaxation regime, and the molecular picture of DTD gave a good approximation for the actual chain motion.[20] In contrast, for entangled six-arm star PI, the DTD relationship failed for a dominant part of the terminal relaxation.[21] Specifically, the observed viscoelastic relaxation was slower than that expected for the DTD process.

This failure of the DTD molecular picture for the star chains suggests that the terminal relaxation of the star chain, i.e., the relaxation of the portion of the star arm near the branching point (BP), occurs before the the CR-equilibration (prerequisite of DTD) for this portion is completed: Since the portion near BP is mostly entangled with quickly relaxing portions near the free ends of the arms, the dynamic situation for the former

* To whom correspondence should be addressed.

10.1021/ma010147q CCC: $20.00
Published on Web 06/26/2001

portion is similar to the situation for long, dilute probe chains[20] entangled with much shorter matrix chains. Extensive experiments indicated that such probes relax with the CR mechanism.[8] This seems to be the case also for the portion of the star arm near BP.

However, we here remember that the DTD relationship ($\mu(t) \cong [\Phi(t)]^2$) for the star chains was derived under the assumption of short-ranged BP fluctuation (with amplitude $< a'$). Although this assumption sounds reasonable, there still remains a small but nonnegligible possibility that the failure of this relationship observed for the six-arm star PI is due to breakdown of this assumption.

For this problem, we have examined viscoelastic and dielectric properties for a series of star PI chains having the same arm molecular weight M_a but different arm number q (= 4−15). Since the entropic penalty for large-amplitude BP fluctuation increases with increasing q, the DTD relationship should become valid for large q *if* the breakdown of the above assumption was the main reason for the failure observed for $q = 6$. Thus, we examined this relationship for the series of star PI chains and found that the relationship was invalid for those chains to nearly the same extent irrespective of the q value. This result indicates that the failure of the DTD picture is intrinsically related to the star chain dynamics, enabling us to discuss the DTD criteria for the star and linear chains in relation to their $\Phi(t)$ data. These results are presented in this paper.

2. Theoretical Section

2.1. Expression of the Dielectric Relaxation Function. For the monodisperse q-arm star chain having noninverted type-A dipoles in each arm, the polarization $\mathbf{P}(t)$ at the time t is proportional to a sum of vectors $\mathbf{R}_\alpha(t)$ that start from the star-branching point (BP) toward the free end of αth arm ($\alpha = 1, 2, ..., q$).[21] The normalized dielectric relaxation function $\Phi(t)$ is given by an autocorrelation of the polarization at equilibrium;[22,23] $\Phi(t) = \langle \mathbf{P}(t)\cdot\mathbf{P}(0)\rangle/\langle \mathbf{P}^2\rangle$ (= 1 at $t = 0$) with $\langle ... \rangle$ representing an ensemble average. Thus, for the q-arm star with the arms having independent Gaussian conformations at equilibrium, $\Phi(t)$ is expressed as[21]

$$\Phi(t) = \frac{1}{qN_a a^2} \sum_{\alpha,\alpha'=1}^{q} \langle \mathbf{R}_\alpha(t)\cdot\mathbf{R}_{\alpha'}(0)\rangle \quad \text{for } q\text{-arm stars} \tag{1}$$

Here, a is a size of the entanglement segment, and N_a is the number of these segments per each arm ($N_a a^2 = \langle\{\mathbf{R}_\alpha(0)\}^2\rangle$).

The dynamic dielectric constant $\epsilon'(\omega)$ and dielectric loss $\epsilon''(\omega)$ at an angular frequency ω are given by the Fourier transformation of $\Phi(t)$[8,23]

$$\epsilon'(\omega) - i\epsilon''(\omega) = \epsilon_\infty - \Delta\epsilon \int_0^\infty \frac{d\Phi(t)}{dt} \exp[-i\omega t]\, dt \quad (i = \sqrt{-1}) \tag{2}$$

Here, ϵ_∞ is the high-frequency dielectric constant, and $\Delta\epsilon$ is the dielectric relaxation intensity (for the global motion of the star chain).

Experiments indicated that star chains exhibit a distribution of dielectric relaxation modes.[21,24] Thus, for convenience, $\Phi(t)$ is expressed in terms of a *dielectric* relaxation spectrum $\{g_p, \tau_p\}$ as[21,24]

$$\Phi(t) = \sum_{p\geq 1} g_p \exp[-t/\tau_p] \tag{3}$$

Here, g_p (satisfying $\sum_p g_p = 1$) represents the normalized intensity of the pth dielectric mode having the relaxation time τ_p. Correspondingly, $\epsilon'(\omega)$ and $\epsilon''(\omega)$ are also expressed in terms of $\{g_p, \tau_p\}$ (cf. eqs 2 and 3). The results are conveniently summarized for the normalized dielectric constant $\{\epsilon_0 - \epsilon'(\omega)\}/\Delta\epsilon$ (ϵ_0 = static dielectric constant) and normalized dielectric loss $\epsilon''(\omega)/\Delta\epsilon$[8,21,24]

$$\frac{\epsilon_0 - \epsilon'(\omega)}{\Delta\epsilon} = \omega^2 \sum_{p\geq 1} g_p \frac{\tau_p^2}{1 + \omega^2\tau_p^2}, \qquad \frac{\epsilon''(\omega)}{\Delta\epsilon} = \omega \sum_{p\geq 1} g_p \frac{\tau_p}{1 + \omega^2\tau_p^2} \tag{4}$$

2.2. Expression of Viscoelastic Relaxation Function. For the entangled star chain subjected to a small step shear strain γ (in the linear viscoelastic regime), the relaxation modulus $G(t)$ in long time scales exclusively reflects decay of orientational anisotropy of the entanglement segments with time.[7,8,25,26] This decay is described by an orientation function

$$S(n,t;\alpha) = \frac{1}{a^2}\langle u_x^\alpha(n,t) u_y^\alpha(n,t)\rangle \tag{5}$$

Here, $u_\xi^\alpha(n,t)$ ($\xi = x, y$) is the ξ component of the bond vector $\mathbf{u}^\alpha(n,t)$ of nth entanglement segment in αth arm at the time t, and the x and y directions are chosen as the shear and shear−gradient directions.

The normalized viscoelastic relaxation function, $\mu(t) = G(t)/G_N$ with G_N being the entanglement plateau modulus, is simply expressed in terms of the orientation function[7,8]

$$\mu(t) = \frac{3}{\gamma}\frac{1}{qN_a}\sum_{\alpha=1}^{q}\sum_{n=1}^{N_a} S(n,t;\alpha) \quad (=1 \text{ at } t = 0) \tag{6}$$

The normalized storage and loss moduli, $G'(\omega)/G_N$ and $G''(\omega)/G_N$, are given by the Fourier transformation of this $\mu(t)$[8,26]

$$\frac{G'(\omega)}{G_N} + i\frac{G''(\omega)}{G_N} = i\omega \int_0^\infty \mu(t) \exp[-i\omega t]\, dt \quad (i = \sqrt{-1}) \tag{7}$$

(In eq 6, we have assumed affine deformation of the chain at $t = 0$ and utilized a corresponding initial condition, $S(n,0;\alpha) = \gamma/3$. If we use the Doi−Edwards initial condition,[7] $S(n,0;\alpha) = 4\gamma/15$ for $\gamma \ll 1$, the prefactor $3/\gamma$ in eq 6 is replaced by $15/4\gamma$. However, this difference does not introduce any change in the DTD relationship explained below.)

2.3. DTD Relationship between μ and Φ. As noted from eqs 5 and 6, the viscoelastic $\mu(t)$ reflects the isochronal orientational anisotropy of respective entanglement segments. In contrast, the dielectric $\Phi(t)$ corresponds to orientational correlation of two entanglement segments at separate times 0 and t; cf. eq 1. (Note that the end-to-end vector of αth arm included in eq 1 is written in terms of $\mathbf{u}^\alpha(n,t)$ of the entanglement segment as $\mathbf{R}_\alpha(t) = \Sigma_n \mathbf{u}^\alpha(n,t)$.)

Thus, the same global motion of the chain is differently averaged in $\mu(t)$ and $\Phi(t)$. This difference enables us to reveal detailed features of the chain dynamics through comparison of viscoelastic and dielectric properties.[8,20,21,27,28] Specifically, for the monodisperse star chains examined in this paper, $\mu(t)$ and $\Phi(t)$ should satisfy a particular relationship when the successive entanglement segments in each arm are mutually equilibrated through their constraint release (CR) motion and the tube dilates accordingly.[21] Under an *assumption* that the star-branching point (BP) fluctuates with an amplitude smaller than the dilated tube diameter, we can write this DTD relationship in a simple form[21]

$$\mu(t) = [\Phi(t)]^{1+d} \cong [\Phi(t)]^2 \quad (d = 1-1.3) \qquad (8)$$

Here, d is the dilation exponent close to unity. For convenience of later discussion of the DTD mechanism, the derivation of this relationship is summarized in the Appendix.

If the above assumption of short-ranged BP fluctuation is valid and *if* the tube for the star chain actually dilates, viscoelastic and dielectric data of the chain should satisfy eq 8. Consequently, the failure of eq 8 (observed for six-arm star PI[21]) strongly suggests that the tube does not effectively dilate because of incomplete CR-equilibration. However, there still remains a small but nonnegligible possibility that the breakdown of that assumption led to the failure of eq 8 (even when the tube actually dilates).

This possibility can be examined for the star chains having identical M_a but different q. The BP fluctuation is associated with shrinkage of one arm and elongation of the remaining $q - 1$ arms. Thus, the entropic penalty for the BP fluctuation increases with increasing q, resulting in suppression of this fluctuation for large q.[29]

As noted from this argument, eq 8 should become valid for large q *if* the breakdown of the assumption of short-ranged BP fluctuation is the main cause of the failure of eq 8. Consequently, the above possibility can be ruled out if eq 8 fails to the same extent for the star PI chains of various q. This is the fundamental strategy of our test of the DTD picture presented in this paper.

3. Experimental Section

3.1. Materials. A series of star *cis*-polyisoprene (PI) samples having the same arm molecular weights M_a ($= 35.5 \times 10^3 \cong 7M_e$; M_e = entanglement spacing) and different arm numbers q (= 4, 6, 9, and 15) were anionically synthesized from the same batch of living arm anions.

First, high vacuum technique (with breakable seals) was utilized to polymerize the linear PI arm anions with *sec*-butyllithium in heptane at room temperature. An aliquot, terminated with methanol, was taken to characterize the arm; M_a ($= M_w$) $= 35.5 \times 10^3$ and $M_w/M_n = 1.02$. GPC (CO-8020 and DP-8020, Tosoh) combined with a law-angle laser-light scattering (LALS) photometer (LS-8000, Tosoh) was utilized for this characterization. The eluent was THF, and monodisperse linear PI samples[20,21,30] were utilized as the elution standards.

The remaining arm anions were divided into three reaction flasks (in a vacuum) to separately synthesize the star PI samples with $q = 4$, 6, 9, and 15. The star samples with $q = 4$ and 6 were prepared via coupling of the arm anions with prescribed amounts (≅90% equimolar) of tetra- and hexafunctional couplers, bis(dichloromethyl silyl)ethane and bis(trichloro silyl)ethane, respectively. The crude products were repeatedly fractionated from benzene/methanol mixtures to remove the excess (unreacted) arms and recover the monodisperse star samples.

Table 1. Characteristics of Star PI Samples[a]

q[b]	$10^{-3}M_w$[c]	M_w/M_n[d]
4	145	1.02
6	208	1.02
9	313	1.03
15	524	1.05

[a] All samples were prepared from the same batch of living arm anion and had the same M_a ($=35.5 \times 10^3$). [b] The number of arms q was evaluated as M_w/M_a. The rounded q values shown in Table 1 are very close to the M_w/M_a ratios of respective star PI. [c] Determined from LALS combined with GPC. [d] Determined from elution calibration of GPC. (LALS-GPC analysis gave M_w/M_n values smaller than those shown in Table 1.)

The star samples with $q = 9$ and 15 were prepared via end-modification of the living arm anions with an equimolar of divinylbenzene (dianionic end-crosslinker) and successive coupling with bis(trichloro silyl)ethane (≅90% equimolar to the anions). The crude product exhibited bimodal GPC−LALS peaks corresponding to the stars with $q = 9$ and 15. This product was thoroughly fractionated from benzene/methanol mixtures to recover these star samples.

The molecular characteristics of the star PI samples, determined with GPC−LALS, are summarized in Table 1. These samples were freeze-dried from benzene solutions containing an antioxidant, butylhydroxytoluene (∼0.1 wt % to the samples), sealed in Ar atmosphere, and stored in a deep freezer until use.

3.2. Measurements. The star PI samples have the type-A dipoles parallel along the arm backbone and their global motion is dielectrically active.[24] For these samples in bulk state, dielectric measurements were conducted with a transformer bridge (1620A, QuadTech) and linear viscoelastic measurements, with a laboratory rheometer (ARES, Rheometrics). A guarded parallel-plate dielectric cell (vacant capacity = 120pF) and a parallel-plate rheometer fixture (diameter = 2.5 cm) were utilized in respective measurements. The time−temperature superposition worked very well for the dielectric and viscoelastic data with the same shift factor a_T. These data were reduced at 40 °C and compared with each other.

4. Results and Discussion

4.1. Overview of Dielectric and Viscoelastic Data. Figure 1 shows the dielectric behavior for the series of well-entangled star PI chains having identical M_a ($\cong 7M_e$) and different q (= 4, 6, 9 and 15). For convenience of later comparison with viscoelastic data, the dielectric data are presented in a normalized form, $\{\epsilon_0 - \epsilon'\}/\Delta\epsilon$ and $\epsilon''/\Delta\epsilon$ plotted against ω; cf. eq 4. (The dielectric intensity $\Delta\epsilon$ utilized in this normalization was evaluated from the ϵ'' data as $\Delta\epsilon = (2/\pi)\int\epsilon''\, d(\ln \omega)$, where the integration was conducted in the ω range for the global relaxation.)

The dielectric relaxation seen in Figure 1 is exclusively attributed to the global motion of the star PI chains. (The relaxation due to local segmental motion occurs at high ω not covered here.) The ω dependences of $\{\epsilon_0 - \epsilon'\}/\Delta\epsilon$ and $\epsilon''/\Delta\epsilon$ are nearly the same for the star PI chains of various q. In particular, the dependences are indistinguishable for $q = 4$ and 6. The dielectric mode distribution of the well-entangled star PI chains, reflected in this dependence, is broader than that of linear PI chains, as pointed out previously.[21,24]

This mode distribution is conveniently described by the dielectric relaxation spectrum $\{g_p, \tau_p\}$; see eq 4. This spectrum is required in our later test of the DTD relationship. Thus, we determined the spectrum from the $\epsilon''/\Delta\epsilon$ data. (Details of this determination are

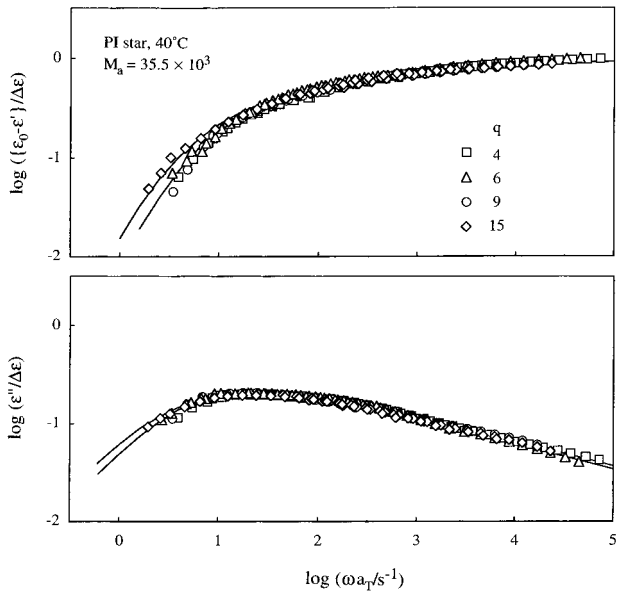

Figure 1. Normalized dielectric data at 40 °C obtained for the star PI chains having identical M_a ($\cong 7M_e$) and various q (= 4, 6, 9, and 15). The solid curves indicate the $\{\epsilon_0 - \epsilon'\}/\Delta\epsilon$ and $\epsilon''/\Delta\epsilon$ of the chains with $q = 6$ and 15 recalculated from the dielectric spectra.

explained later in relation to this test.) In Figure 1, the solid curves indicate the $\{\epsilon_0 - \epsilon'\}/\Delta\epsilon$ and $\epsilon''/\Delta\epsilon$ recalculated from the spectra obtained for the star PI with $q = 6$ and 15. These curves agree with the data very well, indicating satisfactory accuracy in the determination of the spectra. Similar agreement was obtained also for the star PI with $q = 4$ and 9.

For the star PI chains with $q = 4$, 6, 9, and 15, the normalized viscoelastic moduli G'/G_N and G''/G_N are shown in Figure 2. The dominant part of the viscoelastic relaxation, seen at $\omega < 10^3$ s^{-1}, hardly has a contribution from the fast rubber-to-glass transition and reflects the global chain motion.

Extensive experiments indicated that the viscoelastic mode distribution of well-entangled star chains is much broader than the distribution of linear chains.[8,24] This is the case also for our star PI, for which the mode distribution is observed through the ω dependence of the moduli (Figure 2). This distribution is almost identical for the star PI with $q = 4$ and 6 and becomes a little broader at low ω for the star PI with larger q (= 9 and 15). Similar broadening is noted also for the viscoelastic data of star polybutadienes reported by Adams et al.[31] This moderate broadening of the mode distribution may be partly related to suppression of the branching-point fluctuation for large q. (Multiarm stars with $q > 24$ exhibit an extra slow mode that reflects the spatial ordering due to a hard-core-like interaction between densely branching points of neighboring stars.[32−34] However, for our stars with $q \leq 15$, this extra slow mode negligibly contributes to the G^* data.)

Here, we note that the dielectric mode distribution (Figure 1) changes with q less prominently compared to the viscoelastic mode distribution. This difference may reflect the intrinsic difference of the viscoelastic and dielectric properties, the former representing the isochronal orientational anisotropy while the latter detecting the orientational correlation at two separate times.

4.2. Test of DTD Relationship. With the aid of eqs 3 and 7, the DTD relationship (eq 8) obtained under the

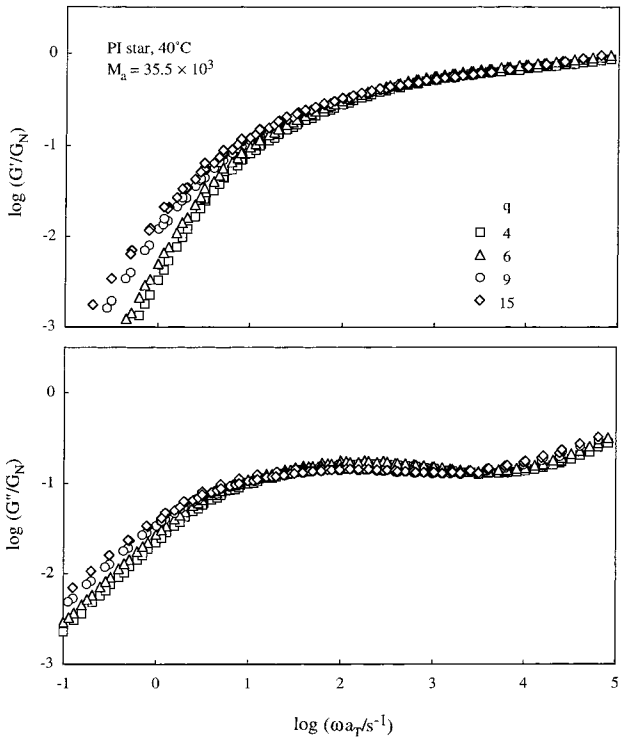

Figure 2. Normalized viscoelastic moduli at 40 °C obtained for the star PI chains having identical M_a ($\cong 7M_e$) and various q (= 4, 6, 9, and 15).

assumption of short-ranged BP fluctuation can be rewritten for the normalized moduli, G'/G_N and G''/G_N. For the smallest possible dilation exponent, $d = 1$, the result is simply written in terms of the dielectric spectrum $\{g_p, \tau_p\}$[21]

$$\frac{G'(\omega)}{G_N} + i\frac{G''(\omega)}{G_N} = \sum_{p,k\geq 1} h_{pk}\frac{\omega^2\tau_{pk}^2 + i\omega\tau_{pk}}{1 + \omega^2\tau_{pk}^2} \quad \text{(for DTD with } d = 1\text{)} \quad (9)$$

with

$$h_{pk} = g_p g_k \quad \text{and} \quad \tau_{pk} = [\tau_p^{-1} + \tau_k^{-1}]^{-1} \quad (10)$$

For a given dielectric $\Phi(t)$, eqs 9 and 10 specify the slowest possible viscoelastic DTD relaxation. (For general cases of $d > 1$, the viscoelastic relaxation is faster than that for $d = 1$; cf. eq 8.)

To test the validity of the above DTD relationship, we assumed a constant logarithmic interval of the dielectric relaxation times, $\log [\tau_p/\tau_{p+1}] = \Delta$ ($p = 1$, 2, ...), to determine the dielectric spectrum from the $\epsilon''/\Delta\epsilon$ data with a previously reported iteration method.[30] For different Δ values (≤ 0.2), we obtained the spectra equally reproducing the $\epsilon''/\Delta\epsilon$ and $\{\epsilon_0 - \epsilon'\}/\Delta\epsilon$ data; cf. solid curves in Figure 1 (for $\Delta = 0.1$) obtained for the star PI with $q = 6$ and 15. This nonuniqueness, the well-known problem in empirical determination of spectra, did not disturb our test of the DTD relationship because the dielectric spectra for different Δ values gave indistinguishable G'/G_N and G''/G_N calculated from eqs 9 and 10.

For the star PI chains with $q = 4$, 6, 9, and 15, Figure 3 compares the G'/G_N and G''/G_N data (unfilled squares and circles) with those calculated from the dielectric spectra obtained for $\Delta = 0.1$ (thick solid and dashed

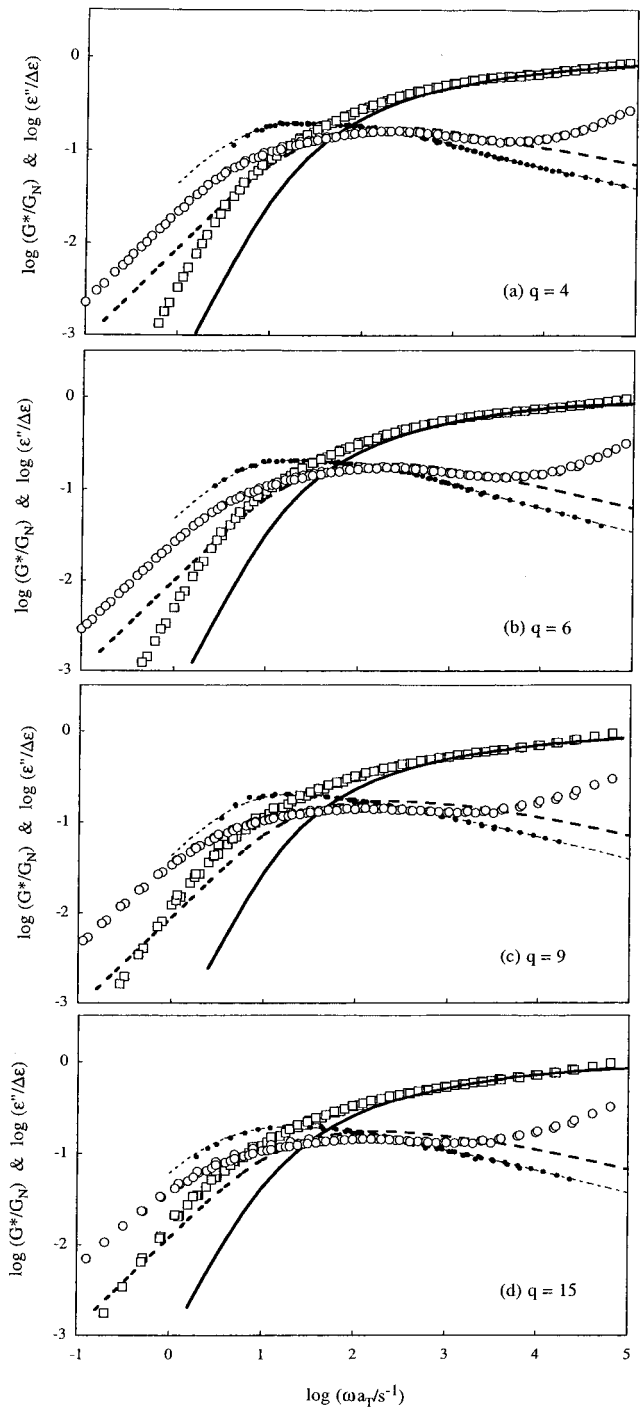

Figure 3. Comparison of normalized viscoelastic moduli G'/G_N (unfilled squares) and G''/G_N (unfilled circles) of the star PI chains with the moduli calculated from the dielectric spectra through the DTD relationship with $d = 1$ (thick solid and dashed curves for G'/G_N and G''/G_N). Small filled circles indicate the normalized dielectric loss $\epsilon''/\Delta\epsilon$ of respective PI chains, and the thin dotted curves are the $\epsilon''/\Delta\epsilon$ recalculated from the dielectric spectra.

curves). The small filled circles indicate the $\epsilon''/\Delta\epsilon$ data, and the thin dotted curve is the $\epsilon''/\Delta\epsilon$ recalculated from the spectra. Differences observed between the $\epsilon''/\Delta\epsilon$ and G''/G_N data unequivocally indicate that the tube is not fixed in space. (In the fixed tube, the chains have $\mu(t) = \Phi(t)$ and their normalized dielectric and viscoelastic losses coincide with each other.[8])

More importantly, Figure 3 demonstrates that the moduli calculated for the case of DTD are different from the data *to nearly the same extent* for the star PI chains of various q. For all PI chains, the observed viscoelastic relaxation is slower than that expected for the case of DTD with $d = 1$. Since this expected relaxation represents the slowest possible viscoelastic DTD relaxation for a given dielectric spectrum, the difference between the observed and calculated moduli seen here unequivocally indicates that the failure of the DTD relationship is *not* due to breakdown of the assumption of the short-ranged BP fluctuation but is intrinsically related to the star chain dynamics.

4.3. DTD Criteria. The DTD process occurs as a result of mutual CR-equilibration of entanglement segments. For the tube diameter to dilate from a to a', successive $(a'/a)^2$ segments need to be equilibrated.[8,12] This CR-equilibration requires a time,[8,21] $\tau^{**} \sim (a'/a)^4 t_w$, where t_w is an average lifetime[6] of the entanglement point: The entanglement lifetime has some distribution, and t_w is an effective CR time-unit that determines the rate of CR-equilibration over $(a'/a)^2$ segments. This lifetime distribution is further discussed in the next section.

The tube can dilate up to a' only in a time scale longer than τ^{**}, meaning that the coarse-graining of the spatial scale (the DTD molecular picture) is intrinsically associated with the coarse-graining of the time scale.[8] This DTD criterion corresponds to that discussed for star/linear blends.[18] In addition, the DTD picture loses its sound meaning when a' becomes comparable with/larger than the chain dimension R ($=N^{1/2}a$ and $N_a^{1/2}a$ for the linear chain and star arm composed of N and N_a entanglement segments, respectively).

These DTD criteria can be cast in inequalities

$$t \geq f\left[\frac{a'(t)}{a}\right]^4 t_w \quad (>t_w) \tag{11}$$

$$\left[\frac{a'(t)}{a}\right]^2 \leq N \text{ (for linear chains), } N_a \text{ (for star chains)} \tag{12}$$

For a quantitative test of the criteria, a numerical prefactor f (set to be unity in the previous, qualitative argument[8,20,24]) has been introduced in eq 11. This f is estimated in the next section.

The DTD picture is valid only in the time scale where eqs 11 and 12 are satisfied. In this time scale, the dielectric $\Phi(t)$ coincides with the survival fraction of the dilated tube (cf. eq A4 in Appendix) and the diameter of this tube is given by $a'(t) \cong a[\Phi(t)]^{-1/2}$.[20,21] Then, eqs 11 and 12 can be rewritten, in terms of experimentally measured/estimated quantities, as

$$\Phi(t) \geq \left[\frac{ft_w}{t}\right]^{1/2} \tag{13}$$

$$\Phi(t) \geq \frac{1}{N} \text{ (for linear chains), } \frac{1}{N_a} \text{ (for star chains)} \tag{14}$$

For representative linear PI ($N = 28$)[20] and six-arm star PI ($N_a = 8.1$)[21] having the largest N and/or N_a among the PI chains so far examined dielectrically, we will examine the validity of the DTD criteria later in Figures 4 and 5. The f and t_w values utilized in this test are estimated below.

4.4. Estimation of f and t_w. For linear chains, the prefactor f and effective entanglement lifetime t_w can

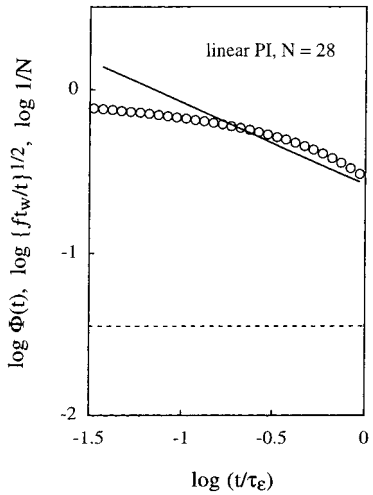

Figure 4. Dielectric relaxation function $\Phi(t)$ of monodisperse linear PI examined in the previous study[20] ($M = 140 \times 10^3$; circles). Solid and dotted lines indicate the factors $\{ft_w/t\}^{1/2}$ (= $2\{0.11\tau_\epsilon/t\}^{1/2}/\pi$) and $1/N$, respectively. The DTD picture is valid in a range of t where $\Phi(t)$ is comparable to/larger than $\{ft_w/t\}^{1/2}$ and $1/N$. For further details, see the text.

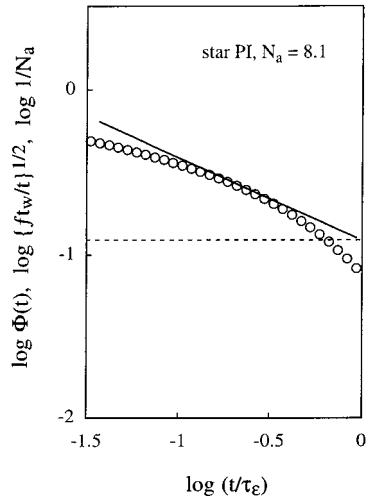

Figure 5. Dielectric relaxation function $\Phi(t)$ of monodisperse, six-arm star PI examined in the previous study[21] ($M_a = 40.7 \times 10^3$; circles). Solid and dotted lines indicate the factors $\{ft_w/t\}^{1/2}$ (= $\{\tau_\epsilon/N_a^2 t\}^{1/2}$) and $1/N_a$, respectively. The DTD picture is valid in a range of t where $\Phi(t)$ is comparable to/larger than $\{ft_w/t\}^{1/2}$ and $1/N_a$. For further details, see the text.

be estimated on the basis of the Graessley model[6] considering the Rouse-like CR process. The global, dielectric CR relaxation time deduced from this model is expressed as[6,8]

$$\tau_{CR,\epsilon} = \frac{4t_w}{\pi^2}N^2 \quad \text{(for linear chain composed of } N \text{ entanglement segments)} \quad (15)$$

The factor $[a'/a]^4$ in eq 11 is the squared number of CR-equilibrated entanglement segments and corresponds to the factor N^2 in eq 15. Thus, the f for linear chains is estimated to be $4/\pi^2$.

For dilute linear probe in linear matrices, the Graessley model relates t_w to the matrix reptation time $\tau_{m,rep}$ as $t_w = (\pi^2/12)^z\tau_{m,rep}/z$, where z represents a number of constraints per entanglement. Adachi et al.[35] examined the dielectric behavior of blends of linear PI and reported that the terminal dielectric relaxation time τ_ϵ of the probe PI can be described by this model with $z \cong 4$. The probe and matrix are identical in monodisperse systems. Thus, the t_w of our monodisperse linear PI ($N = 28$) can be estimated from this z value as $t_w = (\pi^2/12)^z\tau_\epsilon/z = 0.11\tau_\epsilon$.[36]

For star chains, no explicit expression of f is available. In addition, no dielectric data are available for blends of star PI chains, and the t_w of our monodisperse star PI cannot be estimated with the above method. However, viscoelastic experiments for polystyrene blends indicated that the relaxation time of monodisperse star chains with $N_a \leq 6$ is close to the global CR relaxation time.[8,37] This should be the case also for our monodisperse star PI ($N_a = 8.1$), and we may express the measured τ_ϵ in terms of f and t_w as

$$\tau_\epsilon \cong \tau_{CR,\epsilon} = ft_w N_a^2 \quad (16)$$

where the global, dielectric CR time $\tau_{CR,\epsilon}$ is written in a form similar to eq 15. Thus, the product ft_w for our star PI is estimated to be τ_ϵ/N_a^2.

Here, we have to add a few comments for the entanglement lifetime for a probe chain. This lifetime, being determined by the first passage of surrounding chains, should have a distribution along the probe chain contour. The DTD criterion using the single, effective lifetime t_w (eq 13) is approximate in this sense. However, for the dilute linear probe (having the lifetime distribution as suggested by Rubinstein and Colby[38]), the CR model with the single t_w well describes the relaxation data at long times:[8] The slow (global) CR relaxation of the probe results from cooperative motion of many entanglement segments therein, and smearing/averaging of the lifetimes of those segments possibly leads to this validity of the single-t_w model. Correspondingly, we may safely utilize the single-t_w criterion (eq 13) to test the DTD picture for the monodisperse linear chains in long time scales.

The situation would be different for monodisperse star chains. Since the monodisperse star chains have much more widely distributed motional modes compared to the linear chains, the distribution of the entanglement lifetime would be broader for the former. This suggests a limitation of the single-t_w DTD criterion for the star chains.[39] However, the smearing/averaging of the lifetimes explained above is expected also for the star chains *in the long time end of the relaxation*. Thus, in this paper, we utilize this criterion at long times while keeping the limitation at short times in our mind.

4.5. Origin of Failure/Validity of the DTD Picture. On the basis of the DTD criteria (eqs 13 and 14), we can specify why the DTD picture is valid for linear PI in the terminal regime[20] but not for star PI (cf. Figure 3). For the representative linear PI ($N = 28$)[20] and six-arm star PI ($N_a = 8.1$),[21] respectively, Figures 4 and 5 show plots of the dielectric $\Phi(t)$ data, the $\{ft_w/t\}^{1/2}$ factor, and N or N_a against a reduced time t/τ_ϵ. The f and t_w utilized in the plots were estimated in the previous section ($f = 4/\pi^2$ and $t_w = 0.11\tau_\epsilon$ for the linear PI and $ft_w = \tau_\epsilon/N_a^2$ for the star PI), and the terminal dielectric relaxation time τ_ϵ was evaluated from the ϵ' and ϵ'' data as the second-moment average dielectric relaxation time (cf. eq 4)

$$\langle \tau_\epsilon \rangle_w = \frac{[\{\epsilon_0 - \epsilon'(\omega)\}/\omega^2]_{\omega\to 0}}{[\epsilon''(\omega)/\omega]_{\omega\to 0}} = \frac{\sum_{p\geq 1} g_p \tau_p^2}{\sum_{p\geq 1} g_p \tau_p} \qquad (17)$$

(This $\langle \tau_\epsilon \rangle_w$, heavily weighing on slow modes, can be utilized as the terminal τ_ϵ.[8,21,24])

In Figure 4, we can specify a range of t where the DTD criteria are satisfied for the linear PI: $\Phi(t)$ (circles) is comparable with and/or larger than both $\{ft_w/t\}^{1/2}$ (solid line) and $1/N$ (dotted line) in a considerably wide range in the terminal regime, $\tau_\epsilon/8 \leq t$ ($\leq \tau_\epsilon$). Similar results were found for the other linear PI chains (with $N < 28$) examined in this and previous[20] studies. This wide validity of the DTD picture reflects a fact that $\Phi(t)$ of well-entangled linear PI chains has a M-insensitive, narrow mode distribution and relaxes just moderately at $t < \tau_\epsilon$:[20] Since $\Phi(t)$ remains considerably large at $t \leq \tau_\epsilon$ (because of this distribution), the tube diameter can dilate only up to $a'(\tau_\epsilon) = a[\Phi(\tau_\epsilon)]^{-1/2} \cong 1.9a$. In this rather thin tube, the chain can equilibrate itself (through the CR motion) within the given time scale t and thus the tube actually dilates at $t \geq \tau_\epsilon/8$.[40] This result is consistent with the validity of the DTD relationship (eq 8) observed for the viscoelastic G* and dielectric ϵ'' of linear PI in a wide range of ω.[20]

Concerning this point, Figure 4 also indicates that the DTD picture fails at shorter $t < \tau_\epsilon/8$ (cf. circles and solid line). This failure can be related to the obvious limitation of the DTD picture at t being comparable to/shorter than the entanglement lifetime t_w: The CR motion (prerequisite of DTD) is essentially frozen and the tube can never dilate at such short t.

For the star PI, the DTD criteria (eqs 13 and 14) are satisfied in a short time side of the terminal regime, $\tau_\epsilon/10 \leq t < \tau_\epsilon/3$; see Figure 5. At these t, the star arm can quickly equilibrate itself in the enlarged tube expected from the DTD picture, and the tube actually dilates. As explained earlier, our criteria for the star utilizes the single t_w determined from the terminal τ_ϵ (eq 16) and might have the limitation at those short t. However, the DTD relationship between viscoelastic G* and dielectric ϵ'', eqs 8−10 being derived on a general basis *without* the single-t_w approximation, holds at the corresponding high ω; see Figure 3. This results lends support to the above argument about the validity of the DTD picture due to quick CR-equilibration at $\tau_\epsilon/10 \leq t < \tau_\epsilon/3$.

More importantly, Figure 5 demonstrates that $\Phi(t)$ is smaller than $[ft_w/t]^{1/2}$ at longer t ($\geq \tau_\epsilon/3$) where we may safely utilize our single-t_w DTD criteria. Similar results were found for the other star PI (with $N_a \cong 7$; cf. Figure 3). This failure of the DTD picture for the dominant part of the terminal relaxation, being consistent with the violation of eq 8 for G* at low ω (Figure 3), is related to the broad dielectric mode distribution of the star: Because of this broadness, $\Phi(t)$ significantly decays at short t and the tube diameter expected from the DTD picture at long t ($a' \cong a\Phi^{-1/2} \cong 3.6a$ at $t = \tau_\epsilon$) becomes too large to allow the CR-equilibration of the star arm in time.

Concerning this result, we emphasize that the $[ft_w/t]^{1/2}$ factor at a given t/τ_ϵ is considerably larger for the linear PI than for star PI (cf. Figures 4 and 5). Nevertheless, the DTD criterion (eq 13) at long t is more easily satisfied for the linear PI because of its narrow distribution of motional modes (reflected in the dielectric and viscoelastic spectra). Thus, the difference between the linear and star PI chains (success and failure of the DTD picture at long t) is related to the difference in the dynamics of these chains. The star dynamics intrinsically results in the broad motional modes that lead to this failure.

This broadness reflects large differences in the relaxation rates of the portions of arm near the branching point (BP) and free end (FE). In this sense, the monodisperse star chains can be regarded as a blend of slowly relaxing, dilute species (the portion near BP) entangled with a quickly relaxing matrix (the portion near FE). This situation is analogous to that for dilute linear probe chains in much shorter matrix chains. Such probe PI fully relaxes via the CR mechanism, and the DTD picture fails.[20] Thus, the relaxation of the portion of the star arm near BP, observed as the terminal relaxation of the monodisperse star PI, is possibly dominated by the CR mechanism due to fast motion of the portions near FE. This result is consistent with the coincidence of the terminal relaxation time and the global CR time found for monodisperse stars with $N_a \leq 6$.[8,37]

4.6. Comments for Highly Entangled Chains. For the monodisperse linear and star PI having $N \leq 28$ and $N_a \leq 8.1$, the narrow and broad distributions of motional modes result in the success and failure of the DTD picture in the terminal regime. Here, we can ask a question if this is the case for the chains having larger N and N_a.

For linear chains, distributions of slow dielectric and viscoelastic modes are insensitive to N.[8,20] Thus, eqs 13 and 14 are expected to hold in the dominant part of the terminal regime also for $N > 28$; namely, the DTD picture would be valid also for highly entangled linear chains.

For star chains, the mode distributions change with N_a.[5,8,21,24] Specifically, the steady-state compliance J_e of star chains reflecting the viscoelastic mode distribution is described by an empirical equation, $J_e \cong \nu' G_N^{-1} N_a$ with $\nu' = 0.5-0.6$ in a wide range of N_a (<30).[5] From this equation, the normalized terminal viscoelastic relaxation intensity is evaluated to be $\mu(\tau_\epsilon) \cong 1/J_e G_N \cong 1/\nu' N_a$. Thus, for the DTD picture to be valid at long t ($\cong \tau_\epsilon$), the terminal dielectric intensity and the corresponding CR-equilibration time should be given by $\Phi(\tau_\epsilon) \cong [\mu(\tau_\epsilon)]^{1/2} \cong (1/\nu' N_a)^{1/2}$ and $\tau^{**} \cong f[\Phi(\tau_\epsilon)]^{-2} t_w \cong f\nu' N_a t_w$, respectively. However, for this DTD-dominated terminal relaxation for $N_a \gg 1$, the t_w/τ_ϵ ratio would be hardly dependent on N_a (as in the case for linear chains) to give $\tau^{**} > \tau_\epsilon$. Then, the DTD picture is expected to fail for highly entangled stars. Experimental as well as theoretical tests of this naive expectation would be an interesting subject for future work.

5. Concluding Remarks

For a series of monodisperse star PI chains having the same M_a ($\cong 7M_e$) and different arm number q (= 4, 6, 9, and 15), we have compared the viscoelastic and dielectric data to examine the validity of the DTD relationship. For these star PI in the terminal regime, the viscoelastic moduli calculated from the dielectric data through this relationship were different from the data to nearly the same extent, irrespective of the q value. Thus, the assumption of the short-ranged branching-point (BP) fluctuation utilized in derivation of this relationship is not responsible for the observed failure

of the DTD picture. Instead, the failure is intrinsically related to the star chain dynamics associated with broad motional modes, as demonstrated from the analysis of the dielectric $\Phi(t)$ data in relation to the DTD criteria. The analysis also indicated that the success of the DTD picture for the linear chain is related to the narrow distribution of its motional modes.

Acknowledgment. The authors thank T. C. B. McLeish for his invaluable comments about this paper, in particular for the DTD criteria. This work was partly supported by the Ministry of Education, Science, Culture, and Sports, Japan (Grant No. 12650884) and by Japan Chemical Innovation Institute (through the Doi Project for development of Platform for designing high functional materials). Y.M. acknowledges, with thanks, financial support from Hayashi Memorial Foundation for Female Natural Scientists (for fiscal year 2000) and from a JSPS Research Fellowship for Young Scientist (for fiscal year 2001).

Appendix

For monodisperse type-A star chains with each arm being composed of N_a entanglement segments of size a, this Appendix summarizes the derivation of the DTD relationship[21] (eq 8) to specify the underlying assumption.

Survival Fraction of Dilated Tube. In the DTD picture, successive $(a'/a)^2$ entanglement segments are mutually equilibrated to behave as an enlarged segment of size a'.[8,12] The dilated tube is defined as an envelope of these enlarged segments. As a reference for this dilated tube at the time t, every $(a'/a)^2$ segments at the time 0 are combined into an enlarged unit and the *initial*, thick tube is defined as the envelope of these units.

In Figure 6, the dotted tube represents this initial thick tube, and the filled and unfilled circles indicate the entanglement segments at the times 0 and t, respectively. At t, some segments (near the free end of the arm) have escaped from the initial thick tube. The survival fraction $\varphi_\alpha'(t)$ of the dilated tube for the αth arm is defined as a ratio n_α/N_a, where n_α is the number of the entanglement segments of this arm remaining somewhere in the initial thick tube, e.g., in the hatched zone shown in part b of Figure 6. The average survival fraction is defined by[21]

$$\varphi'(t) = \frac{1}{q}\sum_{\alpha=1}^{q} \varphi_\alpha'(t) \qquad \text{(A1)}$$

The mutually equilibrated $(a'/a)^2$ entanglement segments in the dilated tube together behave as an enlarged stress-sustaining unit. Thus, for the case of DTD, the viscoelastic $\mu(t)$ is written as[8,12]

$$\mu(t) = G(t)/G_N = \varphi'(t)\,[N_a'(t)/N_a] \qquad \text{(A2)}$$

Here, $N_a'(t) = a^2N_a/[a'(t)]^2$ is the average number of the enlarged units in each arm at the time t. Equation A2 means that the stress initially sustained by all entanglement segments decays by the factor $[N_a'(t)/N_a]$ due to a decrease of the number of the stress-sustaining units on DTD and by the factor $\varphi'(t)$ due to the escape from the initial thick tube.

In the DTD picture, the fully relaxed portion of the chain is regarded as a solvent[12,13] and φ' is analogous to the polymer concentration. Then, N_a' is expressed as $N_a'(t) = N_a[\varphi'(t)]^d$ with d (= 1−1.3) being the dilation exponent for the entanglement mesh. With this expression, eq A2 becomes

$$\mu(t) = [\varphi'(t)]^{1+d} \quad \text{for stars in the dilated tube} \qquad \text{(A3)}$$

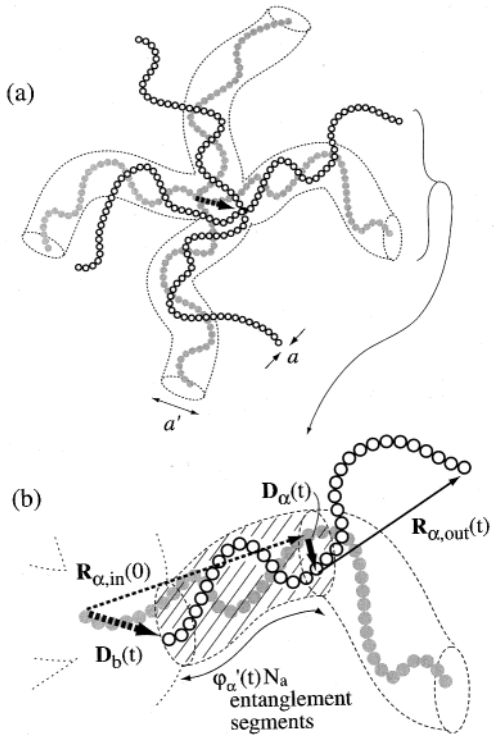

Figure 6. Schematic illustration of the star chain in a dilated tube of diameter $a'(t)$. Filled (gray) and unfilled circles indicate the entanglement segments at times 0 and t. The dotted tube indicates an initial tick tube defined at the time 0, and the hatched zone in part b represents the portion of this initial tick tube surviving at time t. Redrawn, with permission, from ref 21.

DTD Relationship between μ and Φ. The dielectric $\Phi(t)$ of the q-arm star is determined by the correlation of the end-to-end vectors of the arms, $\langle \mathbf{R}_\alpha(t)\cdot\mathbf{R}_{\alpha'}(0)\rangle$ (α, $\alpha' = 1, 2,.., q$); see eq 1. In consideration of this correlation, we can divide the contour of αth arm at the time t in two portions, the outer portion that has escaped from the initial thick tube and the inner portion remaining in this tube. The end-to-end vector of the outer portion, $\mathbf{R}_{\alpha,out}(t)$ (thin solid arrow in part b of Figure 6), is uncorrelated with the initial chain configuration, $\mathbf{R}_{\alpha'}(0)$. This portion has no contribution to $\Phi(t)$.

The inner portion partially preserves its initial memory and contributes to $\Phi(t)$. The end-to-end vector of this portion can be written as $\mathbf{R}_{\alpha,in}(t) = \mathbf{R}_{\alpha,in}(0) + \mathbf{D}_\alpha(t) - \mathbf{D}_b(t)$.[21] Here, $\mathbf{D}_b(t)$ is a displacement of the branching point (BP) in an interval of time between 0 and t (thick dotted arrow in part b of Figure 6), and $\mathbf{D}_\alpha(t)$ is a displacement of the αth arm in the outer edge-plane of the surviving portion of the initial thick tube (thick solid arrow). $\mathbf{R}_{\alpha,in}(0)$ is a vector connecting BP and the entanglement segment in this edge-plane, both at the time 0 (thin dotted arrow).

Since the dilated tube diameter $a'(t)$ represents a length scale over which the lateral motion of the arm can occur in a given time scale t, $\mathbf{D}_\alpha(t)$ has a magnitude

$|\mathbf{D}_\alpha(t)| < a'$ (t) and is not correlated with the initial configuration, i.e., $\langle \mathbf{D}_\alpha(t)\cdot\mathbf{R}_{\alpha'}(0)\rangle = 0$ for $\alpha' = 1, 2, ..., q$.

If BP penetrates into a tube for a particular (α'th) arm to have $|\mathbf{D}_b(t)| > a'$, the other arms are sucked in this tube and correlation between $\mathbf{D}_b(t)$ and $\mathbf{R}_{\alpha'}(0)$ emerges. However, the deeply sucked-in motion (similar to that of a pom-pom[41] in the nonlinear regime) results in loss of conformational entropy and is an unlikely motion at equilibrium (in the linear regime). Thus, the previous work[21] assumed the *short-ranged BP fluctuation* ($|\mathbf{D}_b(t)| < a'$) and the corresponding lack of correlation, i.e., $\langle \mathbf{D}_b(t)\cdot\mathbf{R}_{\alpha'}(0)\rangle = 0$ for $\alpha' = 1, 2,.., q$. (However, thermal fluctuation may result in shallowly sucked-in motion in particular for the stars with small q.)

Thus, under this assumption, we find $\langle \mathbf{R}_\alpha(t)\cdot\mathbf{R}_{\alpha'}(0)\rangle = \langle \mathbf{R}_{\alpha,\mathrm{in}}(t)\cdot\mathbf{R}_{\alpha'}(0)\rangle = \langle \mathbf{R}_{\alpha,\mathrm{in}}(0)\cdot\mathbf{R}_{\alpha'}(0)\rangle = \varphi_{\alpha'}(t)N_a a^2\delta_{\alpha\alpha'}$.[21] Then, eq 1 is rewritten as

$$\Phi(t) = \frac{1}{qN_a a^2}\sum_{\alpha,\alpha'=1}^{q}\langle \mathbf{R}_{\alpha,\mathrm{in}}(0)\cdot\mathbf{R}_{\alpha'}(0)\rangle = \varphi'(t) \quad \text{(A4)}$$

Equations A3 and A4 give the DTD relationship, $\mu(t) = [\Phi(t)]^{1+d} \cong [\Phi(t)]^2$ (eq 8).

References and Notes

(1) Doi, M.; Edwards, S. F. *J. Chem. Soc., Faraday Trans 2* **1978**, *74*, 1789.
(2) Doi, M.; Edwards, S. F. *J. Chem. Soc., Faraday Trans 2* **1978**, *74*, 1802.
(3) Doi, M.; Edwards, S. F. *J. Chem. Soc., Faraday Trans 2* **1978**, *74*, 1818.
(4) Doi, M.; Kuzuu, N. *J. Polym. Sci. Polym. Lett. Ed.* **1980**, *18*, 775.
(5) Pearson, D. S.; Helfand, E. *Macromolecules* **1984**, *17*, 888.
(6) Graessley, W. W. *Adv. Polym. Sci.* **1982**, *47*, 68.
(7) Doi, M.; Edwards, S. F. *The Theory of Polymer Dynamics*, Clarendon: Oxford, England, 1986.
(8) Watanabe, H. *Prog. Polym. Sci.* **1999**, *24*, 1253.
(9) Doi, M. *J. Polym. Sci. Polym. Lett. Ed.* **1981**, *19*, 265.
(10) Doi, M. *J. Polym. Sci. Polym. Phys. Ed.* **1983**, *21*, 667.
(11) Klein, J. *Macromolecules* **1978**, *11*, 852.
(12) Marrucci, G. *J. Polym. Sci. Polym. Phys. Ed.* **1985**, *23*, 159.
(13) Ball, R. C.; McLeish, T. C. B. *Macromolecules* **1989**, *22*, 1911.
(14) Milner, S. T.; McLeish, T. C. B. *Macromolecules* **1997**, *30*, 2159.
(15) Milner, S. T.; McLeish, T. C. B. *Macromolecules* **1998**, *31*, 7479.
(16) Milner, S. T.; McLeish, T. C. B. *Phys. Rev. Lett.* **1998**, *81*, 725.
(17) Viovy, J. L.; Rubinstein, M.; Colby, R. H. *Macromolecules* **1991**, *24*, 3587.
(18) Milner, S. T.; McLeish, T. C. B.; Young, R. N.; Hakiki, A.; Johnson, J. M.; *Macromolecules* **1998**, *31*, 9345.
(19) Stockmayer, W. H. *Pure Appl. Chem.* **1967**, *15*, 539.
(20) Matsumiya, Y.; Watanabe, H.; Osaki, K. *Macromolecules* **2000**, *33*, 499.
(21) Watanabe, H.; Matsumiya, Y.; Osaki, K. *J. Polym. Sci. B Polym. Phys.* **2000**, *38*, 1024.
(22) Cole, R. H. *J. Chem. Phys.* **1965**, *42*, 637.
(23) Riande, E.; Saiz, E. *Dipole Moments and Birefringence of Polymers*; Prentice Hall: Englewood Cliffs, NJ, 1992.
(24) Watanabe, H. *Macromol. Rapid Commun.* **2001**, *22*, 127.
(25) Janeschitz-Kriegl, H. *Polymer Melt Rheology and Flow Birefringence*, Springer: Berlin, 1983.
(26) Ferry, J. D. *Viscoelastic Properties of Polymers*, 3rd ed.; Wiley: New York, 1980.
(27) Watanabe, H.; Yao, M.-L.; Osaki, K. *Macromolecules* **1996**, *29*, 97.
(28) Watanabe, H.; Matsumiya, Y.; Osaki, K.; Yao, M.-L. *Macromolecules* **1998**, *31*, 7538.
(29) For the q arms bound at the branching point (BP), the BP displacement z has a distribution specified by a distribution function $W(z) \sim \exp(-qU(z)/k_BT)$, where k_BT indicates the thermal energy and $U(z)$ is an appropriate free energy increment per arm. This U reflects the entropic penalty for the BP displacement, and the BP fluctuation amplitude is given by $\langle z^2\rangle = \int z^2 W(z)\,dz$. Molecular models suggest different expressions of $U(z)$: For example, the fixed tube models[4,5] suggest $U(z) = \nu' k_B T z^2/N_a a^2$ (with $\nu' =$ constant), and the U suggested from the DTD models[13−15] with the same ν' value is less dependent on z. However, irrespective of details of $U(z)$, the amplitude $\langle z^2\rangle$ decreases with increasing q because of the prefactor q included in $W(z)$.
(30) Yoshida, H.; Adachi, K.; Watanabe, H.; Kotaka, T. *Polym. J.* **1989**, *21*, 863.
(31) Adams, C. H.; Hutchings, L. R.; Klein, P. G.; McLeish, T. C. B.; Richards, R. W. *Macromolecules* **1996**, *29*, 5717.
(32) Vlassopoulos, D.; Pakula, T.; Fytas, G.; Roovers, J.; Karatasos, K.; Hadjichristidis, N. *Europhys. Lett.* **1997**, *39*, 617.
(33) Pakula, T.; Vlassopoulos, D.; Fytas, G.; Roovers, J. *Macromolecules* **1998**, *31*, 8931.
(34) Vlassopoulos, D.; Fytas, G.; Roovers, J.; Pakula, T.; Fleischer, G. *Faraday Discuss.* **1999**, *112*, 225.
(35) Adachi, K.; Itoh, S.; Nishi, I.; Kotaka, T. *Macromolecules* **1990**, *23*, 2554.
(36) Within the generalized tube picture, we may utilize the CLF model[9,10] to relate τ_ϵ of our well-entangled PI to its pure reptation time τ_{rep}; $\tau_\epsilon \cong [1 - N_{DE}^{-1/2}]^2\tau_{rep} \cong 0.7\tau_{rep}$ where, to be consistent, the entanglement segment number N_{DE} (= 35) corresponding to the Doi−Edwards expression of G_N (= $4\rho RT/5M_e$)[7] is utilized. Thus, τ_ϵ of our PI is not significantly different from τ_{rep} and we may utilize $t_w = 0.11\tau_\epsilon$ as a reasonable estimate of the entanglement lifetime for our linear PI: The uncertainty in the $t_w^{1/2}$ factor included in eq 13 due to the use of τ_ϵ instead of τ_{rep} is less than 20% for our linear PI with N_{DE}= 35.
(37) Watanabe, H.; Yoshida, H.; Kotaka, T. *Macromolecules* **1992**, *25*, 2442.
(38) Rubinstein, M.; Colby, R. H. *J. Chem. Phys.* **1988**, *89*, 5291.
(39) Private communication with T. C. B. McLeish.
(40) Note, however, that the monodisperse linear PI chain does not necessarily reptate with its intrinsic diffusivity along the dilated tube:[8,20] This type of reptation requires the equilibration of the chain contour length measured along the dilated tube.[8] This equilibration, involving all entanglement segments in the chain, occurs at $t \geq fN^2t_w \propto N^2\tau_\epsilon$, i.e., not at $t \leq \tau_\epsilon$ for $N \gg 1$.
(41) McLeish, T. C. B.; Larson, R. G. *J. Rheol.* **1998**, *42*, 81.

MA010147Q